Materialia 000 (2018) 1–8

Contents lists available at ScienceDirect

Materialia

journal homepage: www.elsevier.com/locate/mtla

Full Length Article

Investigation of nanoscale twinning in an advanced high manganese twinning-induced plasticity steel

P. Kürnsteiner[a,b,*], C. Commenda[c], E. Arenholz[c], L. Samek[c,d], D. Stifter[a], H. Groiss[a]

[a] Center for Surface and Nanoanalytics (ZONA), Johannes Kepler University Linz, Altenbergerstraße 69, 4040 Linz, Austria
[b] Department Microstructure Physics and Alloy Design, Max-Planck-Institut für Eisenforschung GmbH, Max-Planck-Straße 1, 40237 Düsseldorf, Germany
[c] voestalpine Stahl GmbH, voestalpine Straße 3, 4031 Linz, Austria
[d] University of Applied Science Upper Austria, Metal Sciences, Stelzhamerstraße 23, 4600 Wels, Austria

ARTICLE INFO

Keywords:
TWIP
Microstructure
Dislocations
EBSD
TEM

ABSTRACT

A twinning induced plasticity (TWIP) steel, developed for automotive applications, was characterized down to the nanoscale to investigate the nature of the strengthening mechanisms. Both tensile-deformed and non-deformed materials were studied by light optical microscopy, X-ray diffraction, electron backscatter diffraction, and transmission electron microscopy. The investigated TWIP steel showed extensive twinning upon deformation. With high-resolution transmission electron microscopy, nano-twins as small as 3 nm in width were observed, and large-angle convergent-beam electron diffraction identified the pole mechanism as one of the twinning mechanisms in this TWIP steel. This study emphasizes that a thoughtful combination of techniques is necessary to fully capture the microstructure of this TWIP steel and explain the origin of superior mechanical properties compared to other TWIP steel grades.

1. Introduction

Advanced High Strength Steels (AHSS) are a class of steels that are in continuously-increasing demand from the automotive industry. This high industrial demand stems from the steel's high mechanical strength at reduced thicknesses, and its light weight that allows for an increase in fuel efficiency (and a corresponding reduction in carbon emissions). Twinning Induced Plasticity (TWIP) steels, being high-Mn steels belong to the second-generation AHSS. They meet the high industrial standards of ductility, toughness and strain hardening that makes them well-suited for complex automotive parts. TWIP steels owe their good combination of high strength and large ductility to deformation twinning that reduce the dislocation mean free path upon deformation. This phenomenon is known as dynamic Hall-Petch effect [1,2].

The TWIP steel investigated in this report was produced by a specially-designed thermomechanical process [3,4], and it exhibits superior mechanical properties compared to other TWIP steel grades. The aim of this study is to reveal the details of the microstructure that may explain these superior mechanical properties. We investigated the macroscopic mechanical response by deformation experiments, and we applied a wide array of characterization techniques to the deformed and non-deformed material: light optical microscopy (LOM), X-ray diffraction (XRD), electron backscatter diffraction (EBSD), conventional transmission electron microscopy (TEM), high resolution (HR) TEM and large-angle convergent-beam electron diffraction (LACBED). The breadth of characterization techniques led to a detailed understanding of the complex structure of the material, from the micrometer range down to the nanometer range. We particularly highlight characterization of the twinning behavior, which is the main source for high strain-hardening in TWIP steels. Furthermore, we apply LACBED to confirm a dislocation mechanism of stacking fault formation in this specific steel grade. Both aspects combine to explain the mechanical response.

2. Material and methods

The chemical composition of the investigated steel grade is 15.8 wt% Mn, 0.79 wt% C and 0.05 wt% Si. The concentrations of all other alloy elements (Al, P, Ti, Nb, N and Cr) are below 0.05 wt %. In previous studies [5,6], different alloying concepts (ranging from 12% to 22% Mn) were investigated and it was shown that the composition given above has a fully austenitic microstructure. Samek et al. [4] presented the specific fabrication process for this steel to achieve excellent mechanical properties with 100% elongation and a tensile strength of 1100 MPa. The steel investigated here reached comparable values of (total elongation) × (tensile strength).

Tensile mechanical testing (according to the ISO 6892–1 standard) was used to determine the mechanical properties as well as to strain the samples to defined values (strain $\varepsilon = 0.01$, $\varepsilon = 0.02$, $\varepsilon = 0.05$ and

* Corresponding author at: Max-Planck-Institut für Eisenforschung, Max-Planck Straße 1, 40237 Düsseldorf, Germany.
E-mail address: p.kuernsteiner@mpie.de (P. Kürnsteiner).

https://doi.org/10.1016/j.mtla.2018.04.001
Received 27 February 2018; Received in revised form 9 April 2018; Accepted 12 April 2018
Available online xxx

$\varepsilon = rupture$). These strained samples are sometimes referred to as the deformed samples. Samples deformed in the rolling direction (RD) were used for the microstructural investigations.

The samples were etched for 20–30 s with 3–5% Nital and investigated by LOM (Nikon LABOPHOT-2 Type 115), to gain an overview of the sample microstructure.

For XRD measurements, a Bruker Advance D8 with Mo K_α-radiation source was used to verify the full austenitic phase of the samples.

EBSD measurements were performed on a 1540XB Cross Beam scanning electron microscope from ZEISS equipped with an EBSD system from Oxford Instruments running under the Channel5 software. The electrochemical polishing for the EBSD sample surfaces was carried out on a Struers LectroPol-5 polishing system (equipped with a cooling unit for the electrolyte) using ethanol and perchloric acid (5vol%) at −20 °C.

TEM specimens were prepared either by (1) conventional mechanical preparation with final argon ion milling in a Precision Ion Polishing System (PIPS) from Gatan, or (2) electrochemical preparation with the Struers Tenupol-5 twin-jet system using ethanol and perchloric acid as electrolyte. In-depth investigations of the microstructure were carried out with a JEOL JEM-2011 FasTEM at 200 kV. The dedicated convergent-beam electron diffraction (CBED) mode of this instrument was used for the LACBED experiments.

3. Results

3.1. Tensile testing

Mechanical properties of the steel were evaluated by tensile testing experiments. The results of tensile testing along the RD are shown in Fig. 1a using true stress and true strain. The stress–strain curve is apparently not smooth but shows discontinuities and a jerky flow. This serrated yielding is characteristic of high-Mn TWIP steels being deformed at room temperature and can be attributed to dynamic strain aging [7,8].

In order to obtain the strain hardening coefficient, the true-stress-true-strain curve was fitted using a 7th order polynomial function to allow differentiation, as proposed *e.g.* by Barbier et al. [9], which gives an excellent fit to the experimental data in the region of the plastic deformation. The Young's modulus E was found to be 206 GPa by a linear fit of the elastic regime of the stress-strain curve. This results in a shear modulus of $G = 77$ GPa (with a Poisson's ratio of $\nu = 0.33$ [10]), which agrees well with values reported for similar steels [11,12]. The normalized strain hardening coefficient ($d\sigma/d\varepsilon$) is reported in Fig. 1b. The evolution of the curves and the values are in agreement with the literature [9,12–14].

3.2. Characterization of the non-deformed microstructure

At first, LOM was performed on Nital-etched samples in order to gain an overview of the microstructure. A typical result for a non-deformed sample is shown in Fig. 2a. The sample was slightly over–etched, but its microstructure is still clearly visible. The images shows a carbide-free single-phase austenitic microstructure, consisting of grain sizes from 5 to 40 µm. Annealing twins are also visible – some of these have been marked by green arrows. There is no evidence of strain-induced deformation twins (which differ from the annealing twins by crossing through the entire grain) in the light-optical micrographs.

In XRD measurements of non-deformed material, only the face-centered cubic (*fcc*) lattice peaks appear – there is no evidence of additional peaks from other phases (Fig. 2b). Since XRD provides excellent statistics by averaging over extended volumes, this confirms the full austenitic microstructure on a large scale. Small volume fractions of an additional phase might be undetected, however, if the resulting diffraction peaks are near the background level. Therefore, TEM as well as EBSD were applied to further confirm the single-phase austenitic microstructure.

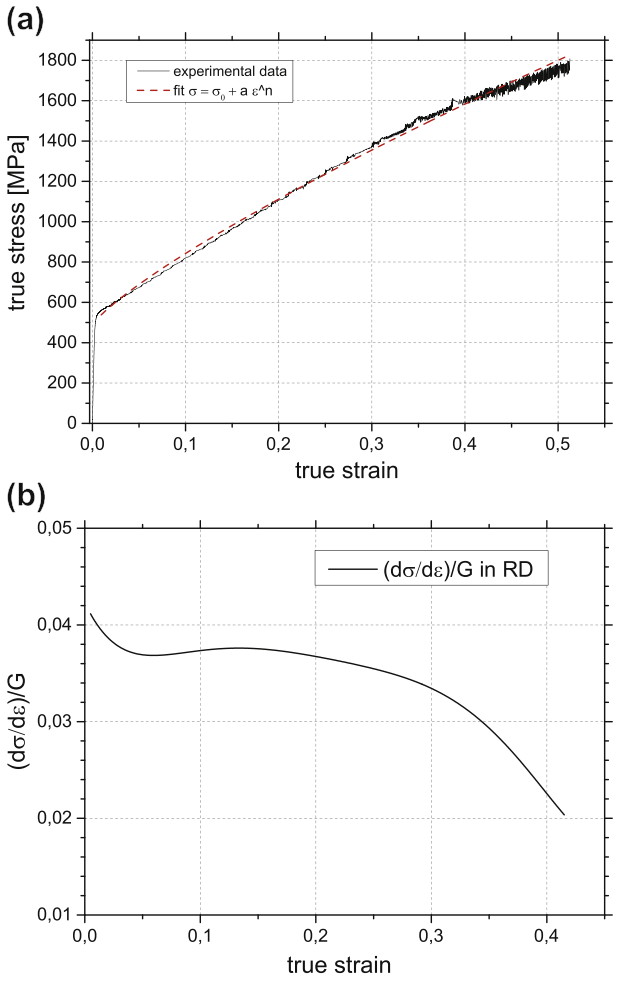

Fig. 1. (a) Stress-strain curve of the investigated steel including a fit according to the Ludwik equation (red dashed curve). (b) Normalized strain hardening derived from the stress strain curve according to the description in the text. (For interpretation of the references to color in this figure legend, the reader is referred to the web version of this article.)

EBSD mappings were performed with 15–30 kV acceleration voltages and step sizes ranging from 2 µm down to 40 nm. On none of the EBSD maps, any indication for martensite formation could be detected.

EBSD experiments were also used to determine the mean grain-size according to the method described by Mingard et al. [15] and following the standard ISO13067. We used electro-polished specimens and an acceleration voltage of 20 kV. A step size of 500 nm was sufficient to resolve even the smaller grains. This value for the step size is approximately 5% of the average grain size (~10 µm), which is well below the recommended [15] value of 10%. With these parameters, we achieved an indexing rate of 90%. We used a dataset of almost two million data points (750 µm x 550 µm) to reach sufficient grain statistics. The result of the EBSD mapping is depicted in Fig. 3a and 3b, which show a selected area of the map.

It is well-documented in literature that if a reasonable grain size cut-off value is used, the map clean-up procedure has relatively little influence on the resulting grain size measurement [15,16]. This is consistent with our experiments with 6457 identified grains: when using a cut-off for grains smaller than 10 pixels as recommended by Mingard et al. [15], 4921 grains remained and the result was a mean circle-equivalent grain diameter of 9.3 µm. We also applied more detailed data clean-up using wild spike extrapolation and extrapolation of unindexed data points, which lead to similar values (9.2 µm), thereby confirming the cut-off value we selected was appropriate. With the EBSD software, the